NANO LETTERS

LETTER

pubs.acs.org/NanoLett

The Graphene–Gold Interface and Its Implications for Nanoelectronics

Ravi S. Sundaram,[†,¶] Mathias Steiner,[*,‡,¶] Hsin-Ying Chiu,[‡] Michael Engel,[§,∥] Ageeth A. Bol,[‡] Ralph Krupke,[§,∥] Marko Burghard,[†] Klaus Kern,[†,⊥] and Phaedon Avouris[‡]

[†]Max-Planck-Institute for Solid State Research, 70569 Stuttgart, Germany

[‡]IBM Thomas J. Watson Research Center, Yorktown Heights, New York 10598, United States

[§]Institut für Nanotechnologie, Karlsruhe Institute of Technology, 76021 Karlsruhe, Germany

[∥]DFG Center for Functional Nanostructures (CFN), 76028 Karlsruhe, Germany

[⊥]Institut de Physique de la Matière Condenseé, Ecole Polytechnique Fédérale de Lausanne, CH-1015, Lausanne, Switzerland

Supporting Information

ABSTRACT: We combine optical microspectroscopy and electronic measurements to study how gold deposition affects the physical properties of graphene. We find that the electronic structure, the electron–phonon coupling, and the doping level in gold-plated graphene are largely preserved. The transfer lengths for electrons and holes at the graphene–gold contact have values as high as 1.6 μm. However, the interfacial coupling of graphene and gold causes local temperature drops of up to 500 K in operating electronic devices.

KEYWORDS: Graphene, gold, semiconductor–metal contact, nano-electronics, nano-optics

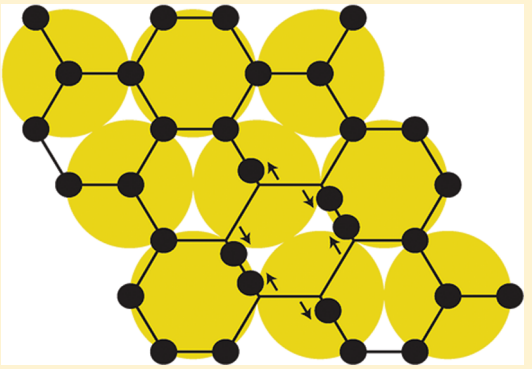

Graphene,[1−3] a monolayer of carbon atoms forming the basal planes of graphite, is currently investigated as a candidate material for high-frequency electronics.[4−6] Its extremely high charge carrier mobilities,[7] supported current densities,[8] and thermal stability[9−14] along with the recent advances in graphene synthesis[15−17] indicate that its use in technology will soon become reality. Metal contacts are essential for interfacing graphene but the surface interaction may modify graphene's electronic structure and doping level[18−20] and impair the performance of future graphene electronics.[21,22] Experimental information of how metal deposition affects fundamental properties like the electric field effect and the electron–phonon coupling in graphene is however lacking. Importantly, the charge carrier transfer length across a graphene–metal interface,[23−25] a measure that determines the ultimate scaling limit (pitch) for integrated electronics, has not yet been directly measured.

In this Letter, we report how gold deposition affects the physical properties of graphene. By applying inverted oil-immersion microscopy to functioning graphene electronic devices built on optically transparent substrates, we are able to monitor *in situ* the electronic structure, the electron–phonon coupling, and the charge carrier transfer length in gold-plated graphene as a function of charge carrier density. Furthermore, we investigate how the interfacial coupling of graphene and gold affects the local temperature in operating electronic devices.

For sample fabrication, we grew graphene on copper by chemical vapor deposition,[15] transferred it onto glass substrates and processed it by using standard lithography and etching techniques (for details see the Supporting Information). We deposited gold films with a thickness of 20 nm directly on the graphene sheet to form the contact electrodes (see Figure 1a). A solid polymer electrolyte layer[26] served as a (top) gate and acted as a protective coating. Figure 1b shows the electrical transfer characteristic of such a graphene device. By fitting the experimental data to the model reported in ref 27 (see also the Supporting Information) we extract the following device parameters: the carrier mobility μ = 1400 cm^2 V^{-1} s^{-1}, the residual carrier density n_0 = 2.6 × 10^{12} cm^{-2}, the electrical-resistance ratio R_{max}/R_{min} = 7, and a relatively low contact resistance R_C = 340Ω · μm, attesting to the quality of the graphene–gold interface. Further analysis accounts for the fact that the charge carrier density in the graphene is not a purely linear function of the polymer gate voltage,[26] as shown in the inset of Figure 1b. Details regarding the extraction of charge carrier densities, n, and Fermi energies, E_F, as functions of the top gate voltage are outlined in the Supporting Information.

Received: June 5, 2011
Revised: July 22, 2011
Published: August 02, 2011

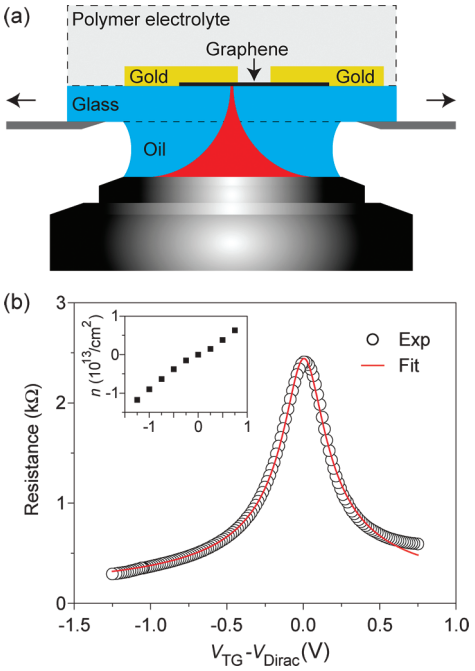

Figure 1. (a) Schematic of a graphene device with a solid-state electrolyte gate built on an optically transparent glass substrate for studying the graphene−gold contact from the underneath with a scanning optical microscope. (b) Electrical transfer characteristics of the electrolyte-gated, optically transparent graphene transistor. The channel length is $L = 1\ \mu$m and the channel width is $W = 2\ \mu$m. (Inset) Dependence of the charge carrier density n on gate voltage $V_{TG} - V_{Dirac}$.

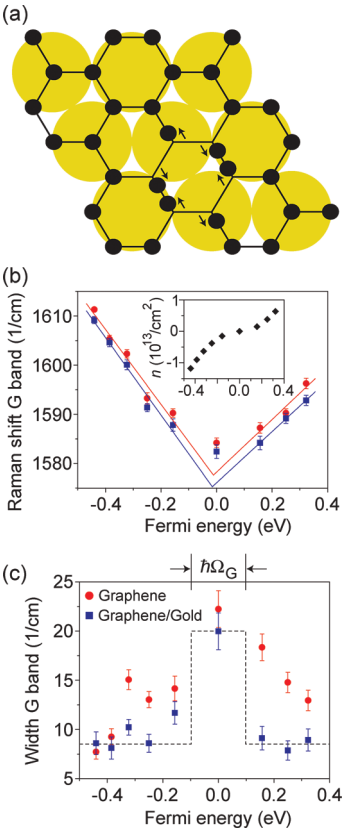

Figure 2. (a) Ideal configuration of graphene on a (111) gold surface derived from calculations based on density functional theory. The Raman-active E_{2g}-symmetry vibration of the carbon atoms (indicated by arrows) gives rise to the G-band. (b) Energy renormalization of the longitudinal optical G-band phonon (symbols, experimental data; solid lines, fit) as function of Fermi energy for graphene (red) and gold-plated graphene (blue), measured on the same graphene sheet. (Inset) Dependence of the charge carrier density n on Fermi energy. (c) Dependence of the G-band line width on Fermi energy. The blockade of the G-band phonon decay for energies $E_F \leq |\pm\hbar\Omega_G/2|$, where Ω_G is the frequency of the G-band phonon, leads to the step-functional behavior around $E_F = 0$. The calculated step function (dotted line) displays a width of $\sigma_{max} = 20\ cm^{-1}$ for $E_F \leq |\pm\hbar\Omega_G/2|$ and $\sigma_{min} = 8.5\ cm^{-1}$ for $E_F > |\pm\hbar\Omega_G/2|$.

We use scanning laser oil-immersion optical microspectroscopy in combination with electrical transport measurements to study the graphene−gold interface in functioning electronic devices (for details see the Supporting Information). As shown in Figure 1a, the optically transparent glass substrate of the device allows for noninvasive and highly sensitive optical measurements of graphene by means of a tightly focused laser beam impinging from the underside of the device. With a suitable scanning unit, we spatially address graphene segments in the device channel and graphene segments under the gold contacts while the charge carrier density in the device is controlled by applying external voltages to gate and gold (source, drain) electrodes.

According to theoretical considerations, the adsorption of gold on graphene is mainly due to the attractive interaction between the d-orbitals of gold atoms and the π-orbitals of the sp^2-hybridized carbon. Calculations based on density functional theory predict a weak chemical bond strength of 0.03 eV per carbon atom,[18] resulting in the idealized packing geometry sketched in Figure 2a. The chemical interaction at the graphene−gold interface could modify the Fermi level, the electronic structure, and the electron−phonon coupling in graphene.

To investigate these changes, we monitor the energy renormalization and the changes in the coupling strength of the longitudinal optical Γ-point phonon in graphene (Raman-active carbon−carbon E_{2g}-symmetry vibration, see Figure 2a) through the Raman G-band[28] at 1585 cm^{-1}. Since the energy (Raman shift) of the G-band phonon depends on charge carrier density,[29,30] the micro-Raman measurement allows us to probe locally both the electric field effect and the electron−phonon coupling in graphene as we tune the gate voltage in the device. This way, we spatially differentiate between the gate response of two segments of the same graphene layer, one segment contacted by gold and the other one in the center of the device channel, without gold layer on top.

In Figure 2b, we plot the respective shifts of the Raman G-band as functions of the Fermi-energy E_F. The corresponding charge carrier density n is plotted as function of E_F in the inset. As we tune E_F in the graphene device by sweeping the top gate voltage across the charge neutrality point, we find that the shift of the G-band in both graphene segments (i.e., with and without gold on top) changes at about the same rate. The best fits to the data in the gold-plated graphene segment deliver (52.1 ± 0.9) cm^{-1} eV^{-1} for $E_F > 0$ and (79 ± 7) cm^{-1} eV^{-1} for $E_F < 0$, respectively. This demonstrates that the electronic structure of graphene, including the charge neutrality (Dirac) point, is preserved in the gold-plated graphene segment. Electron and hole densities in the gold-plated graphene segment (under the contact; even 2 μm away from the contact edge) reach the same

dx.doi.org/10.1021/nl201907u |Nano Lett. 2011, 11, 3833–3837

high values as in the polymer-gated graphene segment (in the device channel). Further data analysis (for details see the Supporting Information and ref 29) reveals that the electron−phonon couplings M_Γ of the longitudinal optical Γ-point phonon in both graphene segments (i.e., with and without gold on top) are identical within experimental error, evidencing the weakness of the perturbation induced by the gold deposition. The best fit to the data obtained in the gold-plated graphene segment delivers $M_\Gamma = (14 \pm 2)$ eV · Å^{-1} for $E_F > 0$ while we obtain $M_\Gamma = (17 \pm 5)$ eV · Å^{-1} for $E_F < 0$, which is in agreement with results obtained for mechanically exfoliated, high-quality graphene.[29,30]

The absence of a horizontal displacement of the two curves in Figure 2b, or the fact that the minima of the two curves coincide at zero Fermi energy, attests to the absence of significant Fermi-level shifts (doping) associated with gold deposition. On the basis of the model reported in ref 18 and our experimental data, we estimate an average distance of 3.2 Å between the gold and graphene layers, close to the theoretical equilibrium separation of 3.3 Å. We attribute the frequency offset of 2 cm^{-1} between the two curves in Figure 2b to a residual, charge-density independent damping of the in-plane, E_{2g} carbon−carbon vibration caused by the gold adsorption (see Figure 2a).

The similar Raman G band widths (around 20 cm^{-1}) observed at the charge neutrality point in the two graphene segments (see Figure 2c) as well as their similar gate dependence demonstrate that the decay pathways of optical phonons in graphene[31] are only weakly affected by the deposition of gold. Landau-damping of the G phonon decay into electrons and holes[29,30] becomes manifest in a step-like functional form of the G-bandwidth around $E_F = |\pm\hbar\Omega_G/2|$, where Ω_G is the frequency of the G-band phonon and is even more pronounced in the gold-plated graphene segment. This indicates that the gold layer might screen potential heterogeneities, for example, due to trapped charges, in the dielectric substrate that could lead to local perturbations of the electron−phonon coupling in graphene.

An important figure of merit is the charge carrier transfer length along a semiconductor−metal interface, L_T, a measure that determines the electrical contact resistance R_c.[32] Scaling the contact width below L_T will reduce the efficiency of charge carrier injection at the graphene−gold interface and increase R_c. According to theory, the electrostatic potential along the graphene−metal interface decays exponentially, $\Phi(x) = \Phi_0 \exp\{-x/L_T\}$, and its 1/e-value defines L_T (for details, see ref 24 and the Supporting Information). We use photocurrent microscopy to measure the transfer length L_T at the graphene−gold contact. In photocurrent microscopy of graphene,[33,34] the closed-circuit photocurrent is proportional to the local potential gradient, $I_{PC}(x) \propto \Phi'(x)$, that separates optically excited charge carriers. An exponential tail fit to the measured photocurrent signal $I_{PC}(x) \propto \Phi'(x) = \Phi'_0 \exp\{-x/L_T\}$ provides the desired L_T-values.

In Figure 3a, we plot cross sections taken from photocurrent scan images at the graphene−gold contact in two different carrier regimes. We find that, despite variations in the vicinity of $|x| <$ 500 nm near the contact edges and residuals away from the contact edges, the photocurrent amplitude decays exponentially within the gold contact. In Figure 3b, we plot the experimental L_T-values obtained as a function of charge carrier density adjusted by the gate. The L_T-values for electrons and holes are symmetrically distributed with respect to the charge neutrality

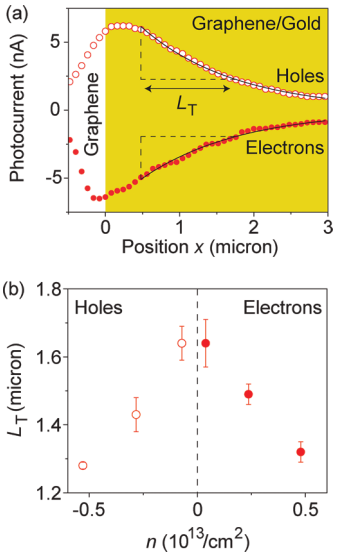

Figure 3. (a) Closed-circuit photocurrent amplitudes measured along the gold−graphene contact for two representative charge carrier densities: $n = -5.3 \times 10^{12}$ cm^{-2} (hole doping, rings) and $n = 4.8 \times 10^{12}$ cm^{-2} (electron doping, circles). The characteristic gold−graphene charge carrier transfer length L_T derived from exponential tail fits (solid lines) is also indicated; the position of the contact edge is at $x = 0$. (b) Dependence of the gold−graphene charge carrier transfer length L_T on charge carrier density n.

point with values as high as 1.6 μm. Since the contact resistance is proportional to L_T, the results imply the occurrence of a contact resistance maximum at the charge neutrality (Dirac) point, in qualitative agreement with the reported gate dependence of the contact resistance in chromium-graphene,[21] titanium-graphene[35] and palladium-graphene[24] junctions.

While we find that the electronic structure and the optical phonons in graphene are only weakly affected by gold deposition, the thermal coupling mediated primarily by acoustic phonon interactions across the graphene−gold interface may cause considerable temperature effects. These effects could strongly affect electronic device performance and stability. In Figure 4a, we sketch the experimental arrangement for a current-carrying graphene device. The scattering of hot charge carriers in the graphene layer provides a major energy dissipation channel and heats up the device, leading to thermoelectric effects,[25] performance reduction and even device failure.

We use optical microthermometry based on the shift of the Raman 2D band in order to measure the temperature of graphene in the operating device[9] and details can be found in the Supporting Information In Figure 4b, we compare the temperatures obtained in the channel center of the graphene device with the temperatures at the graphene−gold contact as function of the injected electrical dc power $P_{el} = I_{ds} \cdot V_{ds}$. We find that both graphene segments heat up linearly as function of P_{el}, however, at largely different rates, $\Delta_{Channel} = (7.4 \pm 0.6)$ K · cm^2/kW and $\Delta_{Contact} = (2.2 \pm 0.3)$ K · cm^2/kW. The resulting temperature difference ΔT between device channel and contact increases at a rate $\delta(\Delta T) = (5.2 \pm 0.8)$ K · cm^2/kW, giving rise to values as high as $\Delta T = 500$ K (see Figure 4c). Such extreme temperature drops, 25 times larger than values reported for a chromium/palladium−graphene contact,[25] increase the risk of device breakdown.

dx.doi.org/10.1021/nl201907u |*Nano Lett.* 2011, 11, 3833–3837

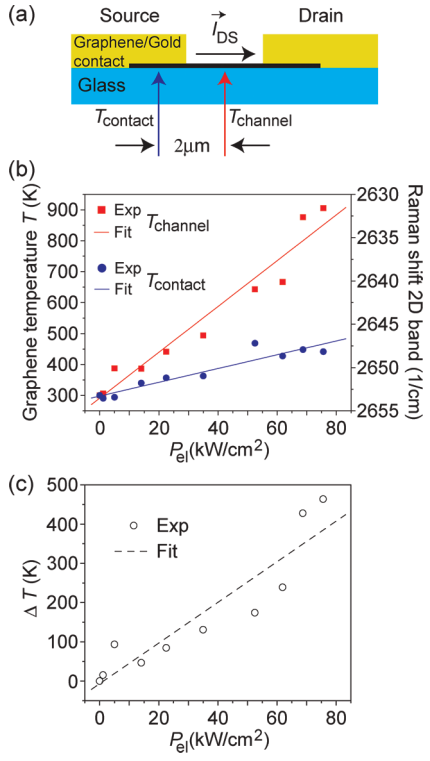

Figure 4. (a) Schematic of a current-carrying, two terminal graphene device without electrolyte polymer layer on top. The gold contacts serve as electrodes for charge carrier injection. The two locations for the temperature measurement at the graphene−gold contact and in the graphene channel are separated by 2 μm. (b) Local temperature of the graphene channel and the graphene−gold contact, respectively, as function of the electrical power P_{el} derived from the measured Raman shift of the 2D-band (symbols). Linear fits (solid lines) deliver different heating rates in the channel center and at the gold contact for the same graphene sheet. (c) Measured temperature difference (rings) between the channel center and the gold contact of the graphene device and a linear fit (dashed line) to the data.

In conclusion, electronic structure, charge neutrality point, and electron−phonon coupling of graphene remain nearly intact upon gold deposition. The charge carrier density at a graphene−gold contact is not pinned and can be tuned by an electrostatic gate. The graphene−gold carrier transfer lengths above 1 μm present severe limitations in the scaling of the gold contact while the thermal coupling at the graphene−gold interface plays an important role in the thermal management during electronic device operation.

■ ASSOCIATED CONTENT

Supporting Information. Additional information. This material is available free of charge via the Internet at http://pubs.acs.org.

■ AUTHOR INFORMATION

Corresponding Author

*E-mail: msteine@us.ibm.com.

Author Contributions

¶These authors equally contributed to this work.

■ ACKNOWLEDGMENT

We thank D. Farmer for discussions and B. A. Ek and T. O. Graham (all IBM T. J. Watson Research Center) for expert technical assistance. M.S. is indebted to H. Kneppe (Deuz, Germany) and A. J. Meixner (Eberhard Karls University, Tuebingen, Germany) for making available several technical drawings.

■ REFERENCES

(1) Geim, A. K. *Science* **2009**, *324* (5934), 1530–1534.
(2) Castro Neto, A. H.; Guinea, F.; Peres, N. M. R.; Novoselov, K. S.; Geim, A. K. *Rev. Mod. Phys.* **2009**, *81* (1), 109.
(3) Avouris, P. *Nano Lett.* **2010**, *10* (11), 4285–4294.
(4) Moon, J. S.; Curtis, D.; Hu, M.; Wong, D.; McGuire, C.; Campbell, P. M.; Jernigan, G.; Tedesco, J. L.; VanMil, B.; Myers-Ward, R.; Eddy, C.; Gaskill, D. K. *IEEE Electron Device Lett.* **2009**, *30*, 650–652.
(5) Lin, Y. M.; Dimitrakopoulos, C.; Jenkins, K. A.; Farmer, D. B.; Chiu, H. Y.; Grill, A.; Avouris, P. *Science* **2010**, *327* (5966), 662.
(6) Schwierz, F. *Nat. Nanotechnol.* **2010**, *5* (7), 487–496.
(7) Bolotin, K. I.; Sikes, K. J.; Jiang, Z.; Klima, M.; Fudenberg, G.; Hone, J.; Kim, P.; Stormer, H. L. *Solid State Commun.* **2008**, *146* (9−10), 351–355.
(8) Moser, J.; Barreiro, A.; Bachtold, A. *Appl. Phys. Lett.* **2007**, *91* (16), 163513–3.
(9) Freitag, M.; Steiner, M.; Martin, Y.; Perebeinos, V.; Chen, Z.; Tsang, J. C.; Avouris, P. *Nano Lett.* **2009**, *9* (5), 1883–1888.
(10) Berciaud, S.; Han, M. Y.; Mak, K. F.; Brus, L. E.; Kim, P.; Heinz, T. F. *Phys. Rev. Lett.* **2010**, *104* (22), 227401.
(11) Chae, D.-H.; Krauss, B.; von Klitzing, K.; Smet, J. H. *Nano Lett.* **2010**, *10* (2), 466–471.
(12) Freitag, M.; Chiu, H.-Y.; Steiner, M.; Perebeinos, V.; Avouris, P. *Nat. Nanotechnol.* **2010**, *5* (7), 497–501.
(13) Bae, M.-H.; Ong, Z.-Y.; Estrada, D.; Pop, E. *Nano Lett.* **2010**, *10* (12), 4787–4793.
(14) Jo, I.; Hsu, I. K.; Lee, Y. J.; Sadeghi, M. M.; Kim, S.; Cronin, S.; Tutuc, E.; Banerjee, S. K.; Yao, Z.; Shi, L. *Nano Lett.* **2011**, *11* (1), 85–90.
(15) Li, X.; Cai, W.; An, J.; Kim, S.; Nah, J.; Yang, D.; Piner, R.; Velamakanni, A.; Jung, I.; Tutuc, E.; Banerjee, S. K.; Colombo, L.; Ruoff, R. S. *Science* **2009**, *324* (5932), 1312–1314.
(16) Bae, S.; Kim, H.; Lee, Y.; Xu, X.; Park, J.-S.; Zheng, Y.; Balakrishnan, J.; Lei, T.; Ri Kim, H.; Song, Y. I.; Kim, Y.-J.; Kim, K. S.; Ozyilmaz, B.; Ahn, J.-H.; Hong, B. H.; Iijima, S. *Nat. Nanotechnol.* **2010**, *5* (8), 574–578.
(17) Dimitrakopoulos, C.; Lin, Y.-M.; Grill, A.; Farmer, D. B.; Freitag, M.; Sun, Y.; Han, S.-J.; Chen, Z.; Jenkins, K. A.; Zhu, Y.; Liu, Z.; McArdle, T. J.; Ott, J. A.; Wisnieff, R.; Avouris, P. *J. Vac. Sci. Technol., B* **2010**, *28* (5), 985–992.
(18) Giovannetti, G.; Khomyakov, P. A.; Brocks, G.; Karpan, V. M.; van den Brink, J.; Kelly, P. J. *Phys. Rev. Lett.* **2008**, *101* (2), 026803.
(19) Gierz, I.; Riedl, C.; Starke, U.; Ast, C. R.; Kern, K. *Nano Lett.* **2008**, *8* (12), 4603–4607.
(20) Varykhalov, A.; Scholz, M. R.; Kim, T. K.; Rader, O. *Phys. Rev. B* **2010**, *82* (12), 121101.
(21) Nagashio, K.; Nishimura, T.; Kita, K.; Toriumi, A. *IEEE Int. Electron Devices Meet. (Baltimore)* **2009**, 1–4.
(22) Nouchi, R.; Tanigaki, K. *Appl. Phys. Lett.* **2010**, *96* (25), 253503–3.
(23) Nagashio, K.; Nishimura, T.; Kita, K.; Toriumi, A. *App. Phys. Lett.* **2010**, *97* (14), 143514–3.
(24) Xia, F.; Perebeinos, V.; Lin, Y.-M.; Wu, Y.; Avouris, P. *Nat. Nanotechnol.* **2011**, *6* (3), 179–184.
(25) Grosse, K. L.; Bae, M.-H.; Lian, F.; Pop, E.; King, W. P. *Nat. Nanotechnol.* **2011**, *6* (5), 287–290.
(26) Das, A.; Pisana, S.; Chakraborty, B.; Piscanec, S.; Saha, S. K.; Waghmare, U. V.; Novoselov, K. S.; Krishnamurthy, H. R.; Geim, A. K.; Ferrari, A. C.; Sood, A. K. *Nat. Nanotechnol.* **2008**, *3* (4), 210–215.

(27) Kim, S.; Nah, J.; Jo, I.; Shahrjerdi, D.; Colombo, L.; Yao, Z.; Tutuc, E.; Banerjee, S. K. *Appl. Phys. Lett.* **2009**, *94* (6), 062107–3.
(28) Ferrari, A. C.; Meyer, J. C.; Scardaci, V.; Casiraghi, C.; Lazzeri, M.; Mauri, F.; Piscanec, S.; Jiang, D.; Novoselov, K. S.; Roth, S.; Geim, A. K. *Phys. Rev. Lett.* **2006**, *97* (18), 187401.
(29) Yan, J.; Zhang, Y.; Kim, P.; Pinczuk, A. *Phys. Rev. Lett.* **2007**, *98* (16), 166802.
(30) Pisana, S.; Lazzeri, M.; Casiraghi, C.; Novoselov, K. S.; Geim, A. K.; Ferrari, A. C.; Mauri, F. *Nat. Mater.* **2007**, *6* (3), 198–201.
(31) Bonini, N.; Lazzeri, M.; Marzari, N.; Mauri, F. *Phys. Rev. Lett.* **2007**, *99* (17), 176802.
(32) Schroder, D. K. *Semiconductor Material and Device Characterization*, 3rd ed.; Wiley: Hoboken, NJ, 2006.
(33) Lee, E. J. H.; Balasubramanian, K.; Weitz, R. T.; Burghard, M.; Kern, K. *Nat. Nanotechnol.* **2008**, *3* (8), 486–490.
(34) Mueller, T.; Xia, F.; Freitag, M.; Tsang, J.; Avouris, P. *Phys. Rev. B* **2009**, *79* (24), 245430.
(35) Blake, P.; Yang, R.; Morozov, S. V.; Schedin, F.; Ponomarenko, L. A.; Zhukov, A. A.; Nair, R. R.; Grigorieva, I. V.; Novoselov, K. S.; Geim, A. K. *Solid State Commun.* **2009**, *149* (27−28), 1068–1071.